

# Particle decay and 21 cm absorption from first minihaloes

E. O. Vasiliev<sup>1,2\*</sup> and Yu. A. Shchekinov<sup>2,3†</sup>

<sup>1</sup>*Institute of Physics, Southern Federal University, Stachki Ave. 194, Rostov-on-Don, 344090 Russia*

<sup>2</sup>*Department of Physics, Southern Federal University, Sorge St. 5, Rostov-on-Don, 344090 Russia*

<sup>3</sup>*Special Astrophysical Observatory RAS, Nizhny Arkhyz, 369167 Russia*

Accepted 2006 December 15. Received 2006 April 1; in original form 2006 April 1

## ABSTRACT

We consider the influence of decaying dark matter (DM) particles on the characteristics of 21 cm absorption in spectra of distant radio-loud sources – “21 cm forest” – from minihaloes with masses  $M = 10^5 - 10^7 M_\odot$  virialized at  $z_{vir} = 10$ . We use 1D self-consistent hydrodynamic description to study evolution of minihaloes, and follow up their absorption characteristics from turnaround to virialization. We find that in the presence of decaying dark matter both thermal and dynamical evolution of minihaloes demonstrate significant deviation from those in the model without dark matter decay (standard recombination). We show that optical depth in 21 cm line is strongly suppressed in the presence of decaying particles: for  $M = 10^5 - 10^6 M_\odot$  decaying dark matter with the energy rate deposited in baryonic gas  $\xi_L = 0.59 \times 10^{-25} \text{ s}^{-1}$  – the current upper limit of the energy deposit – decreases the optical depth and the equivalent width by an order of magnitude compared to the standard recombination. Thus additional ionization and heating from decaying DM particles almost “erases” absorption features from minihaloes with  $M = 10^5 - 10^6 M_\odot$  for  $\xi \gtrsim 0.3 \xi_L$ , which consequently considerably decreases the number of strong absorptions: for example, the number of absorptions with the equivalent width  $W_\nu^{obs} \gtrsim 0.3 \text{ kHz}$  at  $z \simeq 10$  decreases more than 2.5 times for  $\xi/\xi_L = 0.3$  and  $\gtrsim 4.5$  times for  $\xi/\xi_L = 1$ . We argue that “21 cm forest” absorptions might be a powerful probe of the presence of decaying dark matter in the early Universe.

**Key words:** early Universe – cosmology: theory – dark matter – diffuse radiation – line: formation - radio lines: general

## 1 INTRODUCTION

A way to study pre-reionization history of the intergalactic medium lies in observation of the redshifted 21 cm line produced in the hyperfine transition of neutral hydrogen (Hogan & Rees 1979; Scott *et al.* 1991; Madau *et al.* 1997). There are at least three techniques to use the 21 cm line for studying this epoch: observations of emission or absorption of the neutral intergalactic medium (IGM) against the cosmic microwave background (CMB) – the 21 cm global signal (Shaver *et al.* 1999; Sethi 2005), statistical studies of the angular distribution of the intensity in the 21 cm line – the 21 cm fluctuations (Tozzi *et al.* 2000; Iliev *et al.* 2002), and measurements of absorption along the line of sight to a distant radio-loud quasar – the “21 cm forest” (Carilli *et al.* 2002; Furlanetto & Loeb 2002). The first two methods provide mapping of the 3D space-redshift features of the IGM, whereas the latter works only along line of sight, i.e. pro-

vides a 1D probe. A physical distance corresponded to the angular resolution of existing and future radiotelescopes, such as e.g. LOFAR<sup>1</sup>, is about one megaparsec. Therefore only huge structures, such as for example, HII regions formed by stellar clusters and quasars, the large scale cosmic web structure, are possible to detect. Instead, by measuring the absorption features along redshift we can resolve small scale structure, e.g. individual minihaloes, galaxies, stellar HII regions (Kumar *et al.* 1995; Bagla *et al.* 1997; Furlanetto & Loeb 2002; Furlanetto 2006; Yue *et al.* 2009; Mack & Wyithe 2011).

Ionizing photons produced by first stellar objects change gas thermal state in minihaloes and their vicinity, and as a consequence, affect the 21 cm absorption features (Yue *et al.* 2009; Xu *et al.* 2011). Similar effect can be expected from other possible sources of ionizing photons, such as decaying dark matter (DM) particles (Sciama 1982; Scott *et al.* 1991; Bharadwaj & Sethi

\* E-mail: eugstar@mail.ru

† E-mail: yus@sfedu.ru

<sup>1</sup> <http://www.lofar.org/index.htm>

1998; Chen & Kamionkowski 2004; Hansen & Haiman 2004; Kasuya & Kawasaki 2004; Kasuya *et al.* 2004; Pierpaoli 2004; Belikov & Hooper 2009), annihilation of dark matter (Chuzhoy 2008; Myers & Nusser 2008; Yuan *et al.* 2010; Cumberbatch *et al.* 2010) and ultra-high energy cosmic rays produced in decay of superheavy dark matter particles with masses  $M_X \gtrsim 10^{12}$  GeV (Berezinsky *et al.* 1997; Birkel & Sarkar 1998; Kuzmin & Rubakov 1998; Doroshkevich & Naselsky 2002; Doroshkevich *et al.* 2003). Previous studies have shown that ionizing background produced by these sources can affect thermal and ionization evolution of the intergalactic medium (Dodelson & Jubas 1994; Biermann & Kusenkov 2006; Shchekinov & Vasiliev 2004; Vasiliev & Shchekinov 2006; Mapelli *et al.* 2006) and influence through it the 21 cm global signal and fluctuations (Furlanetto *et al.* 2006; Shchekinov & Vasiliev 2007; Chuzhoy 2008; Myers & Nusser 2008; Yuan *et al.* 2010; Cumberbatch *et al.* 2010; Natarajan A. & Schwarz 2009). Recent studies strongly constrain properties of such ionizing radiation sources (Zhang *et al.* 2007; Cirelli *et al.* 2009; DeLope Amigo *et al.* 2009; Peter *et al.* 2010; Zhang *et al.* 2010; Galli *et al.* 2011; Hütsi *et al.* 2011), though do not fully exclude them. Therefore, in this paper we focus on how the 21 cm absorption – “21 cm forest” – depends on the decaying dark matter parameters.

The 21 cm forest is supposed to be a signal from numerous minihaloes along line of sight being at different evolutionary states from the turnaround to the virialization, with the absorption features depending on the evolutionary state (Meiksin 2011; Vasiliev & Shchekinov 2012). In several previous studies minihaloes were considered as static objects with fixed dark matter and baryonic profiles (Furlanetto & Loeb 2002; Furlanetto 2006). More recently accretion has been added (Xu *et al.* 2011), and further, the evolutionary effects during the formation of minihaloes have been taken into account (Meiksin 2011; Vasiliev & Shchekinov 2012).

Another aspect important when characteristics of the 21 cm forest are concerned relates to spatial distribution of matter in minihaloes. The dark matter profile is mostly assumed cuspy (Navarro *et al.* 1997). However, according to the observations of local dwarf galaxies the dark matter profile is flatter (Burkert 1995). Recently in several theoretical studies it has been pointed out that the first protogalaxies may also have a flat dark matter profile (Mashchenko *et al.* 2006; Tonini *et al.* 2006; Mikheeva *et al.* 2007). It seems obvious that changes in dark matter profiles result in corresponding changes of the radial distribution of baryonic component inside minihaloes, and consequently, in the 21 cm absorption properties.

In this paper we study the effects of decaying dark matter particles on absorption features of non-static (evolving) minihaloes with a flat dark matter profile. We assume a  $\Lambda$ CDM cosmology with the parameters  $(\Omega_0, \Omega_\Lambda, \Omega_m, \Omega_b, h) = (1.0, 0.76, 0.24, 0.041, 0.73)$  (Spergel *et al.* 2007).

## 2 EVOLUTION OF MINIHALO

To model the evolution of minihaloes we use a one-dimensional Lagrangian code. For dark matter we follow the

description given by Ripamonti (2007). Namely, the dark matter,  $M_{DM} = \Omega_{DM} M_{halo} / \Omega_M$ , is assumed to be enclosed within a certain truncation radius  $R_{tr}$ , inside which the dark matter profile is a truncated isothermal sphere with a flat core of radius  $R_{core}$ . The parameter  $\eta = R_{core} / R_{vir}$  is taken 0.1 for all simulations. Such a description is used to mimic the evolution of a simple top-hat fluctuation (e.g. Padmanabhan 1993). In order to describe time evolution of the truncation radius we make use of the approximation formula for a top-hat density perturbation in the form proposed by Tegmark *et al.* (1997).

For simulations of baryonic component we use a 1D Lagrangian scheme similar to that described by Thoul & Weinberg (1995). As a standard resolution we used 1000 zones over the computational domain, and found a reasonable convergence.

Chemical and ionization composition include a standard set of species: H, H<sup>+</sup>, H<sup>-</sup>, He, He<sup>+</sup>, He<sup>++</sup>, H<sub>2</sub>, H<sub>2</sub><sup>+</sup>, D, D<sup>+</sup>, D<sup>-</sup>, HD, HD<sup>+</sup> and *e*. The corresponding reaction rates are taken from (Galli & Palla 1998; Stancil *et al.* 1998). Energy equation includes radiative losses typical in primordial plasma: Compton cooling, recombination and bremsstrahlung radiation, collisional excitation of HI (Cen 1992), H<sub>2</sub> (Galli & Palla 1998) and HD (Flower 2000; Lipovka *et al.* 2005).

We start our one-dimensional simulations at redshift  $z = 100$ . The initial parameters: gas temperature, chemical composition of gas and other quantities – we have taken from simple one-zone calculations began at  $z = 1000$  with typical values at the end of recombination:  $T_{gas} = T_{CMB}$ ,  $x[\text{H}] = 0.9328$ ,  $x[\text{H}^+] = 0.0672$ ,  $x[\text{D}] = 2.3 \times 10^{-5}$ ,  $x[\text{D}^+] = 1.68 \times 10^{-6}$  (see references and details in Ripamonti 2007, Table 2).

## 3 IONIZATION AND THERMAL HISTORY

The contribution from decaying dark matter is described by the corresponding ionization and heating terms into equations for the ionization and thermal evolution. The ionization rate due to presence of additional ionization sources from decaying particles is written as (Chen & Kamionkowski 2004)

$$I_e(z) = \chi_i f_x \Gamma_X \frac{m_p c^2}{h\nu_c} \quad (1)$$

where  $\chi_i$  is the energy fraction deposited into ionization (Shull & van Steenberg 1985),  $m_p$  is the proton mass,  $f_x = \Omega_X(z) / \Omega_b(z)$ ,  $\Omega_b(z)$ , the baryon density parameter,  $\Omega_X(z)$ , the fractional abundance of decaying particles,  $\Gamma_X$  is the decay rate,  $h\nu_c$ , the energy of Ly-c photons. In general, the ionization history depends on the energy rate deposited in baryonic gas,  $\xi = \chi_i f_x \Gamma_X$  (Chen & Kamionkowski 2004).

The heating rate produced by ionizing photons from decaying dark matter particles can be written in the form (Chen & Kamionkowski 2004)

$$K = \chi_h m_p c^2 f_x \Gamma_X \quad (2)$$

where  $\chi_h$  is the energy fraction depositing into heating (Shull & van Steenberg 1985). By order of magnitude  $\chi_i \sim \chi_h \sim 1/3$  for the conditions we are interested in.

Using the CMB datasets Zhang *et al.* (2007) have constrained the energy rate of the radiatively decaying dark matter as the upper limit  $\xi_L \lesssim 1.7 \times 10^{-25} \text{ s}^{-1}$ . Extending analysis with data of Type Ia supernova, Ly $\alpha$  forest, large scale structure and weak lensing observations have lead DeLope Amigo *et al.* (2009) to stronger constraints:  $\xi_L \lesssim 0.59 \times 10^{-25} \text{ s}^{-1}$ . It is worth noting that all datasets favour long-living decaying dark matter particles with the lifetime  $\Gamma_X^{-1} \gtrsim 100 \text{ Gyr}$  (DeLope Amigo *et al.* 2009). Further improvement is expected from the Planck satellite. In this paper we consider the decaying dark matter with  $\xi \leq \xi_L = 0.59 \times 10^{-25} \text{ s}^{-1}$  and compare results with the standard recombination scenario, i.e.  $\xi = 0$ .

#### 4 SPIN TEMPERATURE

The two processes: atomic collisions and scattering of ultraviolet (UV) photons, couple the HI spin temperature and the gas kinetic temperature (Field 1958; Wouthuysen 1952)

$$T_s = \frac{T_{CMB} + y_a T_k + y_c T_k}{1 + y_a + y_c} \quad (3)$$

here  $T_{CMB}$  is the CMB temperature,  $y_c, y_a$  are the functions determined by the collisional excitations and the intensity of the UV resonant photons

$$y_a = \frac{P_{10} T_*}{A_{10} T_k}, \quad y_c = \frac{C_{10} T_*}{A_{10} T_k} \quad (4)$$

$T_* = 0.0682 \text{ K}$  is the hyperfine energy splitting,  $A_{10} = 2.87 \times 10^{-15} \text{ s}^{-1}$  is the spontaneous emission rate of the hyperfine transition,  $C_{10} = k_{10} n_H + \gamma_e n_e$  is the collisional de-excitation rate by hydrogen atoms and electrons, the photon induced de-excitation rate is negligible, for  $k_{10}$  we use the approximation by Kuhlen *et al.* (2006), for  $\gamma_e$  we take the approximation from Liszt (2001),  $P_{10}$  is the indirect de-excitation rate, which is related to the total Ly $\alpha$  scattering rate  $P_a$  (Field 1958)

$$P_{10} = 4P_a/27, \quad (5)$$

where  $P_a = \int cn_\nu \sigma_\nu d\nu$ ,  $n_\nu$  is the number density of photons per unit frequency range,  $\sigma(\nu)$  is the cross-section for Ly $\alpha$  scattering (Madau *et al.* 1997).

Additional ionizations produced by decaying dark matter deposit into Ly $\alpha$  photon budget due to recombination. In our calculations we do not take into account the UV pumping, firstly because such deposit is minor in comparison with the atomic collisions for the decaying dark matter parameters and redshifts considered here (see Figure 2 in Shchekinov & Vasiliev 2007). Secondly, contribution from Ly $\alpha$  background produced by star-forming minihaloes is small due to the rarity of first stellar objects at redshifts  $z = 10 - 15$ . Moreover, it can be readily shown that in order to compete contribution from atomic and electron collisions to HI spin temperature UV energy flux has to be unacceptably high:  $F_{Ly\alpha} \gtrsim 0.1 \text{ erg s}^{-1} \text{ cm}^{-2}$  for gas with  $T \sim 200 \text{ K}$  and  $n \sim 1 \text{ cm}^{-3}$  at  $z \sim 10$ .

#### 5 RESULTS

Stellar and quasi-stellar sources of ionizing radiation begin to form at redshifts  $z < 20$ . They heat the surround-

ing gas through photoionization, which then emits in 21 cm with a patchy, spot-like distribution on the sky. Instead, the decaying particles illuminate and heat the IGM homogeneously by X-ray photons normally produced in decays (Chen & Kamionkowski 2004). Such photons have mean free path length much longer than the typical distance between minihaloes,  $d \sim 30(1 + z/20) \text{ kpc}$ . Therefore in minihaloes the ionization and heating rates due to decays of dark matter particles can be taken equal to the rates in the IGM background.

#### 5.1 Dynamics of minihaloes

Heating from decaying dark matter weakens the accretion rate of baryons on to the minihaloes. Therefore, in comparison with the evolution of minihaloes in the standard scenario one can expect smaller baryon mass and higher temperature within the virial radius of a minihalo. The influence of decaying particles depends on the minihalo mass and the rate of the decay energy deposited in gas,  $\xi$ .

Here we consider evolution of minihaloes within the mass range  $M = 10^5 - 10^7 M_\odot$  virialized at  $z_v = 10$ . Our choice of the redshift of virialization is caused by the fact that at lower redshifts the effects of reionization begin to play dominant role and thus contaminated contribution from decaying dark matter. On the other hand, at higher redshifts the number of bright radio objects which can serve as background sources where minihaloes can imprint becomes low. In the mass range we focus on the three characteristic masses:  $M = 10^5, 10^6$  and  $10^7 M_\odot$  for the following reasons. It has been found that inside minihaloes with  $M \simeq 2 \times 10^6 M_\odot$  the star formation can potentially occur at  $z \simeq 10$  (see also Ripamonti 2007), in the sense that such minihaloes collapse at  $z_{vir} = 10$ , i.e. the gas density in the most inner shell reaches around  $10^8 \text{ cm}^{-3}$  and grows up further. Minihaloes with lower masses cannot cool efficiently and form stars at  $z \sim 10$ . Therefore the first mass considered here  $M = 10^5 M_\odot$  represents in general the low-mass end of non-starforming minihaloes. The second value  $M = 10^6 M_\odot$  cannot also collapse at  $z \sim 10$ , but it is close to the critical mass  $M \simeq 2 \times 10^6 M_\odot$ , and represents qualitatively correct characteristics of 21 cm absorptions in the range of masses of marginally star-forming minihaloes. The third value is  $M = 10^7 M_\odot$ : such minihaloes collapse (and therefore can form stars) even before the virialization redshift, namely, at  $z \simeq 11$ . Thus, we study evolution and absorption characteristics of the minihaloes, which from one side can remain dark after virialization ( $M = 10^5 - 10^6 M_\odot$ ) and from the other form first stars ( $M = 10^7 M_\odot$ ).

##### 5.1.1 Evolution of minihaloes with $M = 10^5 M_\odot$ and $10^6 M_\odot$ .

Figures 1-2 show radial profiles of number density (upper), temperature (middle) and velocity (lower panels) in minihaloes  $M = 10^5, 10^6 M_\odot$  virialized at  $z_{vir} = 10$ , for the three redshifts  $z = 15.5, 12$  and  $10$  (from left to right panels, correspondingly).

For  $M = 10^5 M_\odot$  the virial temperature about 500 K is close to the one in the IGM heated by decaying DM particles with  $\xi/\xi_L \gtrsim 0.1$ . At the turnaround state (left panels)

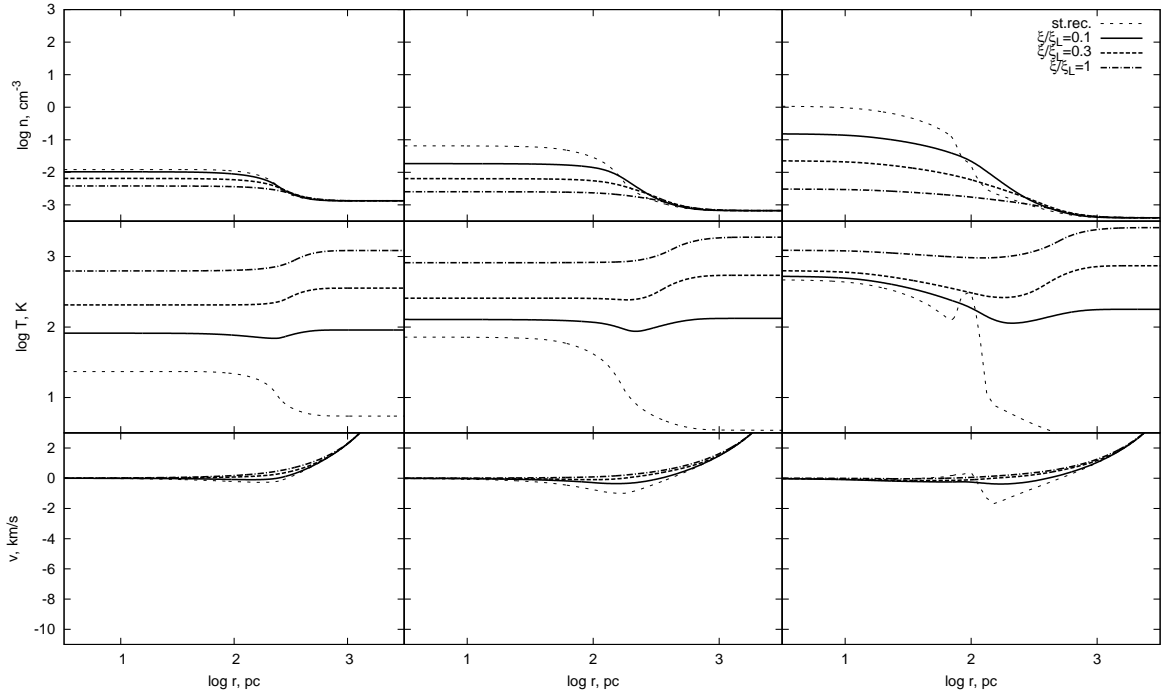


**Figure 1.** The radial density (upper), temperature (middle) and velocity (lower panels) profiles of a halo  $M = 10^5 M_\odot$  virialized at  $z_{\text{vir}} = 10$  are shown at redshifts  $z = 15.5, 12$  and  $10$  (from left to right panels, correspondingly) in the standard recombination model (dots) and in the presence of decaying dark matter with  $\xi/\xi_L = 0.1, 0.3, 1$  (solid, dash and dot-dashed lines, correspondingly), where  $\xi_L = 0.59 \times 10^{-25} \text{ s}^{-1}$ . Note that in the presence of decaying dark matter gas almost ceases collapse into the minihalo potential well.

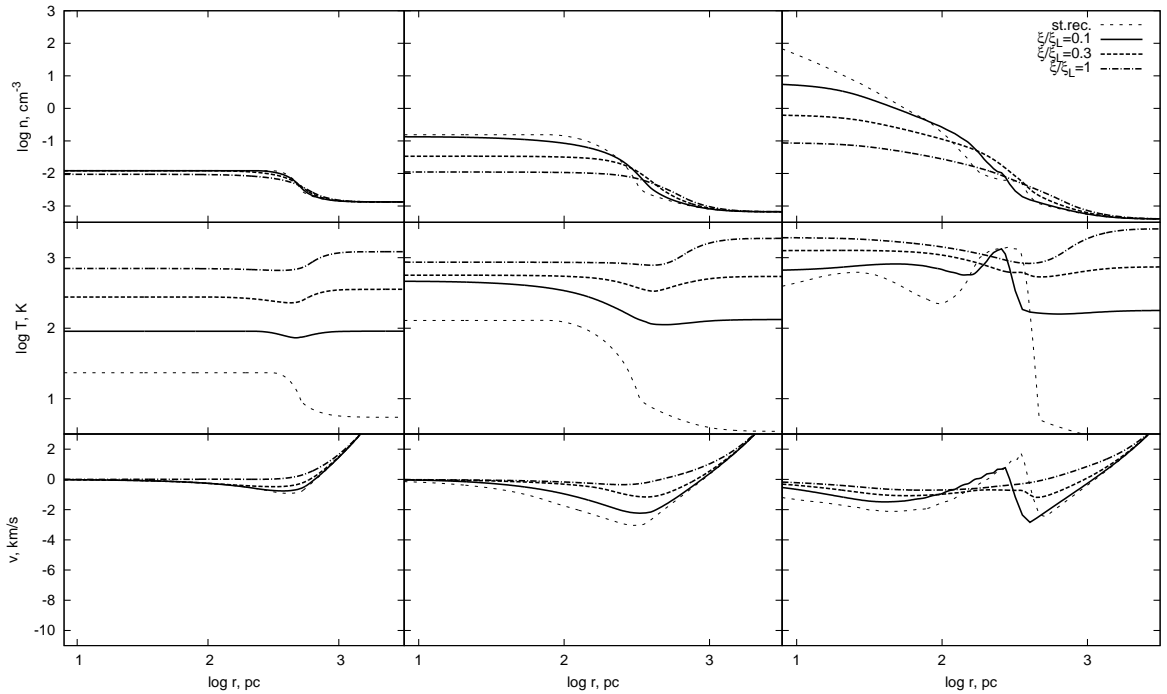


**Figure 2.** The radial density (upper), temperature (middle) and velocity (lower panels) profiles of a halo  $M = 10^6 M_\odot$  virialized at  $z_{\text{vir}} = 10$  are shown at redshifts  $z = 15.5, 12$  and  $10$  (from left to right panels, correspondingly) in the standard recombination model (dots) and in the presence of decaying dark matter with  $\xi/\xi_L = 0.1, 0.3, 1$  (solid, dash and dot-dashed lines, correspondingly), where  $\xi_L = 0.59 \times 10^{-25} \text{ s}^{-1}$ . Note the absence of the accretion (virial) shock for  $\xi/\xi_L \gtrsim 0.3$  (right lower panel), whereas for the lower  $\xi/\xi_L$  the profiles tend to those in the standard recombination model.

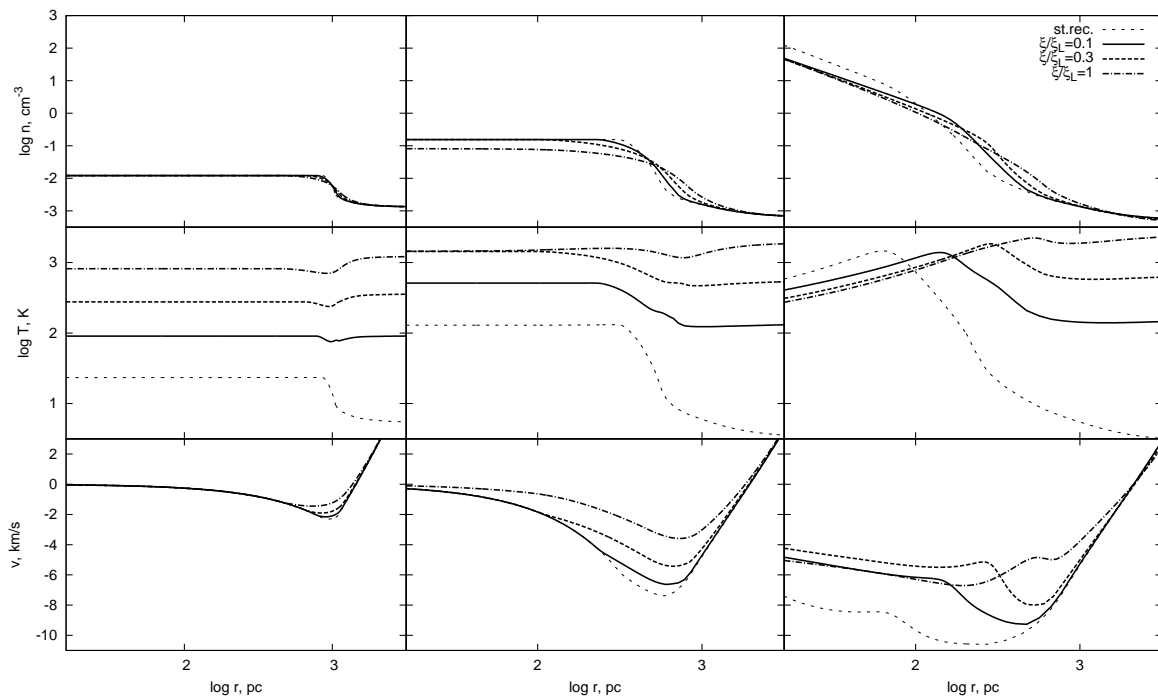


**Figure 3.** The radial density (upper), temperature (middle) and velocity (lower panels) profiles of a halo  $M = 10^7 M_\odot$  virialized at  $z_{\text{vir}} = 10$  are shown at redshifts  $z = 15.5, 12$  and  $11$  (from left to right panels, correspondingly) in the standard recombination model (dots) and in the presence of decaying dark matter with  $\xi/\xi_L = 0.1, 0.3, 1$  (solid, dash and dot-dashed lines, correspondingly), where  $\xi_L = 0.59 \times 10^{-25} \text{ s}^{-1}$ . Note that the velocity profiles demonstrate a stable gas collapse in the potential well of the dark halo. The density and velocity profiles for all considered  $\xi/\xi_L$  are close to those in the standard scenario, though the temperature profiles  $\xi/\xi_L$  demonstrate appreciable difference.

temperature profiles differ significantly from the standard one: namely, they show the internal and the external temperatures practically equal due to additional heating from decaying DM particles. Such a high background temperature in the presence of decaying particles can cause stopping gas collapse in the minihalo potential well during further evolution.

At  $z = 12$  (middle panels of Figure 1) the standard model shows obvious gas accretion resulting in an increase of density and temperature. At the same time in models with  $\xi \gtrsim 0.3\xi_L$  gas velocities are non-negative at any radius, so that the baryon content of minihalo does not grow. The density within the plateau  $r \lesssim 100 \text{ pc}$  for  $\xi = \xi_L$  is an order of magnitude lower than in the standard recombination – this is clearly seen on the lower panel of Figure 1. At the virialization this difference in density increases: for low ionization rates  $\xi \lesssim 0.3\xi_L$  the density grows several times compared to that at  $z = 12$ , while for higher  $\xi = \xi_L$  it stays nearly the same. As a result for high ionization rates the deviation from the standard model reaches two orders of magnitude. Practically in the whole range of ionization rates temperature profiles within  $r \lesssim 100 \text{ pc}$  do not deviate significantly from each other, showing a dominance of the decaying DM in heating. The most appreciable difference between the standard recombination and the models with decaying dark matter is the absence of a significant accretion shock wave around  $r \sim 100 \text{ pc}$ . In the standard case such a wave is obviously seen on the right lower panel of Figure 1. Thus the presence

of decaying dark matter prevents collecting baryonic mass in the minihaloes with  $M \simeq 10^5 M_\odot$ .

For  $\xi \gtrsim 0.3\xi_L$  the evolution of minihaloes with  $M = 10^6 M_\odot$  is similar to that with  $M = 10^5 M_\odot$  (the dash and dash-dotted lines in Figure 2). Whereas for lower rate  $\xi$  evolution of  $M = 10^6 M_\odot$  looks closer to the standard recombination model. Note, in particular, the presence of the virial shock for  $\xi = 0.1\xi_L$  (solid lines at the lower row of panels in Figure 2) similar to that in the standard case (dotted line).

### 5.1.2 Evolution of minihaloes with $M = 10^7 M_\odot$ .

For  $M = 10^7 M_\odot$  the density profiles<sup>2</sup> for all  $\xi$  considered here are close to those in the standard recombination scenario (Figure 3). Instead, temperature and velocity profiles demonstrate considerable differences. These differences can be explained by the accretion of warmer intergalactic gas. At the turnaround temperature inside the halo is almost equal to the background value (middle left panel), which is higher than the standard background temperature. At this stage gas has already begun collapsing into the potential well of the dark halo, providing the velocity profiles almost coincided for all  $\xi \lesssim \xi_L$  (lower left panel). In further accretion of warm intergalactic gas the differences between models

<sup>2</sup> As for minihaloes with  $M = 10^7 M_\odot$  the collapse (i.e. the time when gas density in the most inner shell reaches  $10^8 \text{ cm}^{-3}$  and grows further) occurs earlier than formal virialization, we present the results for not later than the collapse redshift, i.e. for  $z = 11$ .



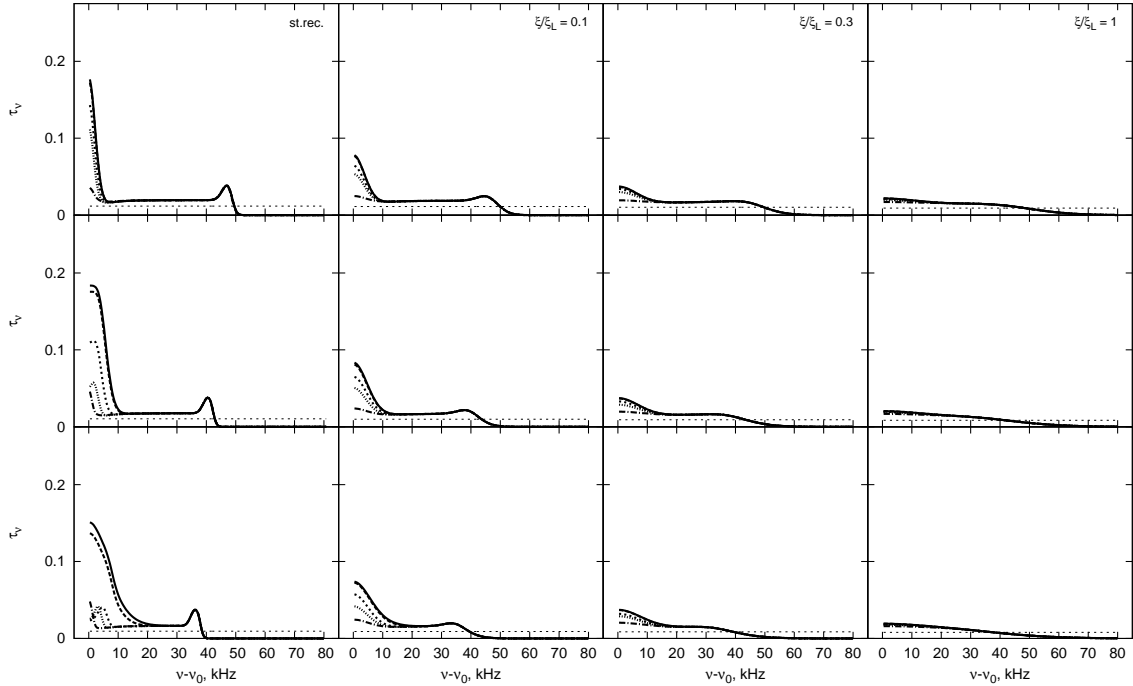


**Figure 4.** Optical depth at the impact parameters  $\alpha = 0.1, 0.3, 1, 1.5, 3r/r_{vir}$  (solid, dash, dot, short dash and dot-dash lines, correspondingly) for a halo  $M = 10^5 M_\odot$  virialized at  $z_{vir} = 10$ , at redshifts  $z = 15.5, 12$  and  $10$  (from top to bottom panels, correspondingly) in the standard recombination model and in the presence of decaying dark matter with  $\xi/\xi_L = 0.1, 0.3, 1$  (from left to right, correspondingly), where  $\xi_L = 0.59 \times 10^{-25} \text{ s}^{-1}$ .

start revealing at  $z = 12$ . Temperature inside the minihalo ( $r \lesssim 500$  pc) becomes considerably higher for the models with decaying particles. The absolute value of the velocity decreases with an increase of the rate  $\xi$ , i.e. baryons collapse slower. At the collapse redshift,  $z \simeq 11$ , differences in the temperature and the velocity profiles for different rates  $\xi$  remain significant in the whole radial range. In all models there the virial shock wave does not appear, the velocity profiles demonstrate stable collapse of gas in the potential well of the dark halo. One can note that the profiles for the models with decaying particles are close each other and to the profile for the standard reionization within  $r \lesssim 200$  pc which corresponds to  $r \lesssim 0.5r_{vir}$ .

The evolutionary differences for minihaloes in the mass range  $M = 10^5 - 10^7 M_\odot$  in the decaying dark matter models are expected to become seen in the HI 21 cm absorption characteristics. In the following sections we consider how the differences manifest in optical depth and equivalent width of the 21 cm absorption.

## 5.2 Optical depth

The optical depth at a frequency  $\nu$  along a line of sight is

$$\tau_\nu = \frac{3h_p c^3 A_{10}}{32\pi k \nu_0^2} \int_{-\infty}^{\infty} dx \frac{n_{HI}(r)}{\sqrt{\pi} b^2(r) T_s(r)} \exp\left[-\frac{[v(\nu) - v_l(r)]^2}{b^2(r)}\right] \quad (6)$$

where  $r^2 = (\alpha r_{vir})^2 + x^2$ ,  $\alpha = r/r_{vir}$  is the impact parameter (a line of sight crosses the minihalo at a distance  $\alpha r_{vir}$  from the centre of the minihalo),  $v(\nu) = c(\nu - \nu_0)/\nu_0$ ,  $v_l(r)$  is the infall velocity projected on the line of sight,  $b^2 = 2kT_k(r)/m_p$  is the Doppler parameter of gas.

Figures 4-6 show the optical depth at several impact parameters,  $\alpha$ , for the haloes with  $M = 10^5, 10^6, 10^7 M_\odot$  at redshifts  $z = 15.5, 12$  and  $10$  (from top to bottom, correspondingly)<sup>3</sup> in the standard recombination model and in the presence of decaying dark matter with  $\xi/\xi_L = 0.1, 0.3, 1$ . The analysis of the 21 cm absorption features of minihaloes in the standard recombination scenario can be found in (Xu *et al.* 2011; Meiksin 2011; Vasiliev & Shchekinov 2012).

### 5.2.1 Line profiles in on-star-forming minihaloes: $M = 10^5 M_\odot$ and $10^6 M_\odot$ .

Minihaloes with  $M = 10^5 M_\odot$  show a small peak in optical depth at  $\nu - \nu_0 \simeq 40$  kHz (Figure 4). This peak emerges from dynamics of the halo: it forms in a narrow external layer of the halo where a non-zero diverging velocity overlaps with a fast decreasing temperature profile –  $b^2(r)$  in the denominator of the exponent (6). The peak weakens in models with decaying DM. Note very weak or lack of dependence of the optical depth at  $\nu - \nu_0 > 10$  kHz on the impact parameter, reflecting the fact that the velocity profiles are flat within

<sup>3</sup> For  $M = 10^7 M_\odot$  the lowest redshift is  $z \simeq 11$ , see Section 5.1 for details.

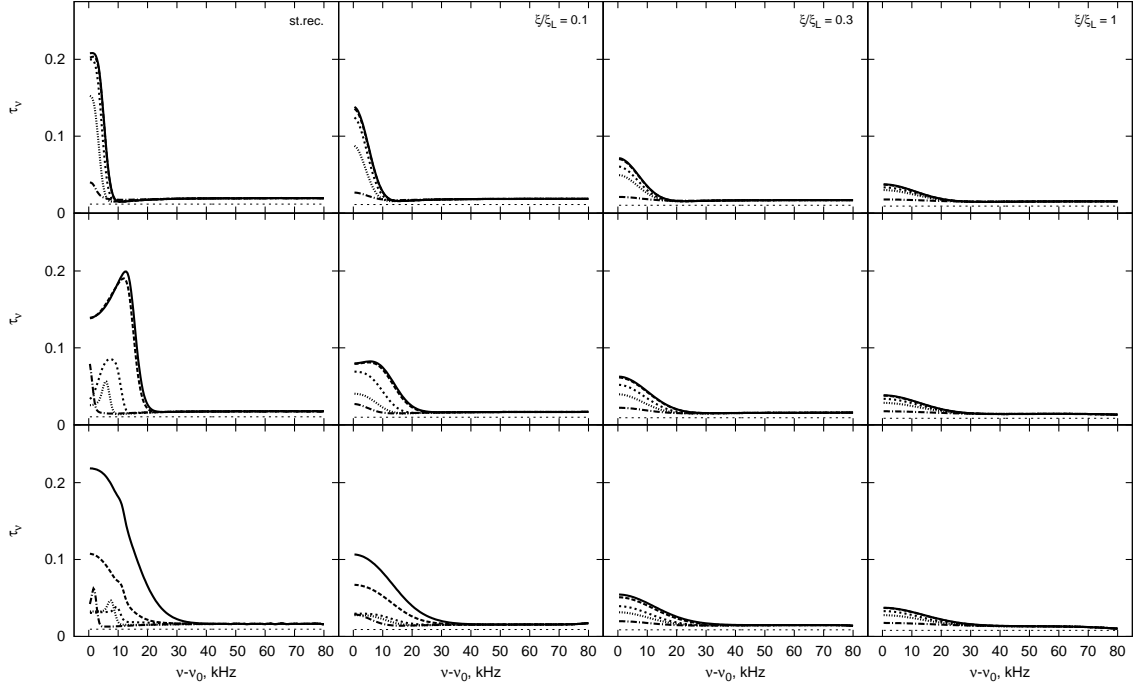


**Figure 5.** The same as in Figure 4, but for a halo with  $M = 10^6 M_\odot$ :  $\alpha = 0.1, 0.3, 1, 1.5, 3r/r_{vir}$  (solid, dash, dot, short dash and dot-dash lines, correspondingly), at redshifts  $z = 15.5, 12$  and  $10$  (from top to bottom).

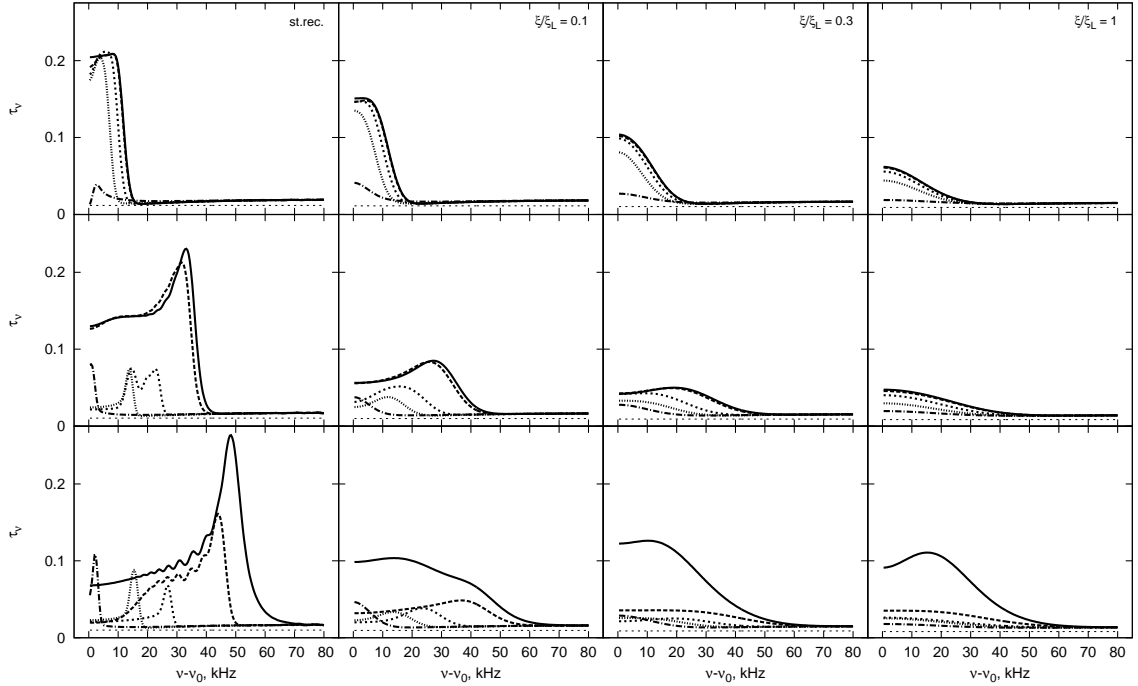


**Figure 6.** The same as in Figure 4, but for a halo with  $M = 10^7 M_\odot$ :  $\alpha = 0.1, 0.3, 1, 1.5, 3r/r_{vir}$  (solid, dash, dot, short dash and dot-dash lines, correspondingly), at redshifts  $z = 15.5, 12$  and  $10$  (from top to bottom).

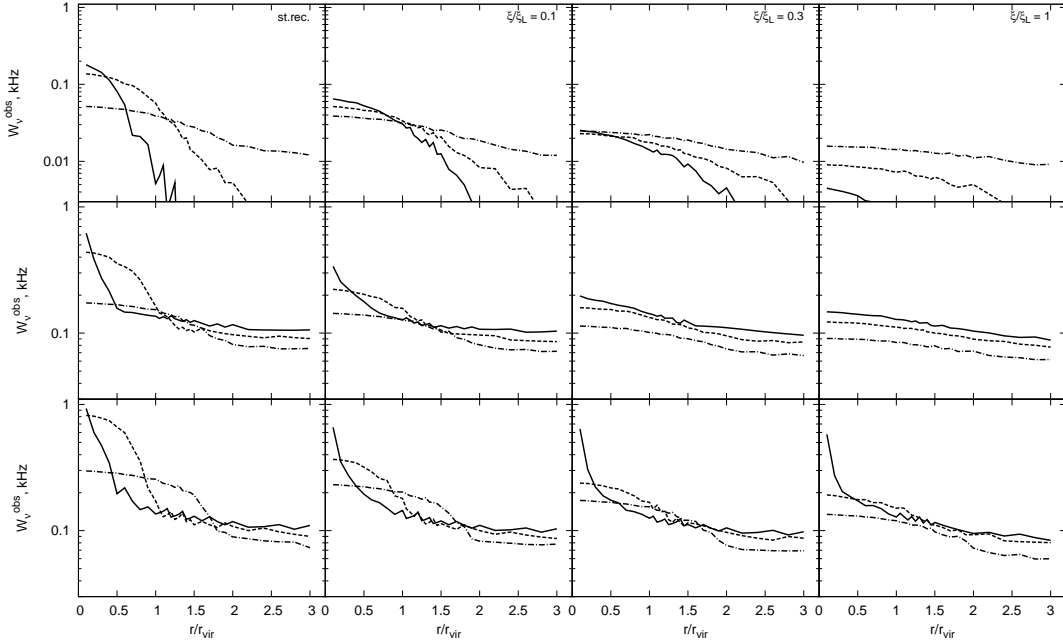


**Figure 7.** The observed equivalent widths for minihaloes with mass  $M = 10^5, 10^6, 10^7 M_\odot$  (from top to bottom) at redshifts  $z = 15.5, 12$  and  $z = z_{\text{vir}} = 10$  (dot-dash, dash and solid lines, correspondingly) in the standard recombination model and in the presence of decaying dark matter with  $\xi/\xi_L = 0.1, 0.3, 1$  (from left to right, correspondingly), where  $\xi_L = 0.59 \times 10^{-25} \text{ s}^{-1}$ . Note that the y-axes are different between panels.

haloes and do not practically depend on the ionization parameter (1). In the standard scenario optical depth drops sharply at higher frequencies,  $\nu - \nu_0 > 50 \text{ kHz}$ , from one side because temperature at the boundary falls down to very low background temperature, and from the other, because velocity at the boundary joins the Hubble flow (such that the numerator in the exponent of (6) increases). In the presence of decaying dark matter the peak at  $\nu - \nu_0 \simeq 40 \text{ kHz}$  is suppressed due to the increase of the background temperature (leading to an increase of denominators both in the exponent and in the integrand of (6)). For higher masses similar peaks are found at higher frequencies, though they contribute little to absorption.

An obvious result is that the presence of decaying dark matter particles heavily suppresses optical depth: for  $M = 10^5 M_\odot$  in the standard recombination scenario optical depth at  $\alpha = 0.1$  reaches  $\sim 0$ , and falls below  $\sim 0.06$  for  $\xi > 0.1\xi_L$ . For  $M = 10^6 M_\odot$  optical depth shows similar dependence, though frequency profiles at  $\alpha > 0.3$  seem in principle distinguishable at lower ionization rates  $\xi \lesssim 0.3\xi_L$  (Figure 5). Thus, the decaying dark matter practically erases 21 cm absorption features from minihaloes with  $M = 10^5 - 10^6 M_\odot$  and the ionization rate higher than  $\xi \gtrsim 0.3\xi_L$ .

Horn-like profiles in  $M = 10^6 M_\odot$  haloes at  $z = 12$  (middle left panel of Figure 5) are due to continuing accretion of atomic hydrogen at these stages – such profiles are first described by Xu *et al.* (2011). They disappear either during further evolution when the halo settles down to a virial state (lower left panel), or in the models with an increase of the decaying dark matter where heating prevents contraction (middle row of panels).

### 5.2.2 Line profiles in star-forming minihaloes: $M = 10^7 M_\odot$ .

In the standard recombination horn-like profiles due to strong accretion in massive haloes around its virialization (Xu *et al.* 2011; Vasiliev & Shchekinov 2012) are clearly seen at  $\alpha \lesssim 0.3$ . More precisely, they origin due to lower spin temperature in the region with the maximum infall velocity as seen from the integrand in (6). Higher infall velocity for a minihalo  $M = 10^7 M_\odot$  shifts maximum of the optical depth towards higher frequencies (cf. the position of the optical depth maximum at  $z = 12$  and  $z = 10$  for e.g.  $\alpha = 0.1$ , see Figure 3).

In general, in the presence of decaying dark matter the accretion rate (i.e. the infall velocity) weakens (see Figure 3), because of warming of the accreting gas. As a consequence the optical depth maximum shifts to lower frequencies and a horn-like dependence of the optical depth almost disappears for  $\xi \gtrsim 0.1\xi_L$ .

### 5.3 Equivalent width

The suppression of the 21 cm line optical depth by decaying DM particles manifests in decrease of the observed line equivalent width determined as  $W_\nu^{\text{obs}} = W_\nu/(1+z)$ , where the intrinsic equivalent width is

$$\frac{W_\nu}{2} = \int_{\nu_0}^{\infty} (1 - e^{-\tau_\nu}) d\nu - \int_{\nu_0}^{\infty} (1 - e^{-\tau_{IGM}}) d\nu \quad (7)$$

where  $\tau_{IGM}$  is the optical depth of the background neutral IGM. Figure 7 demonstrates the observed equivalent width for minihaloes with mass  $M = 10^5, 10^6, 10^7 M_\odot$  at redshifts  $z = 15.5, 12$  and  $10$ , for the standard recombination and in



the presence of decaying dark matter with  $\xi/\xi_L = 0.1, 0.3, 1$ . As expected the equivalent width decreases significantly with an increase of  $\xi$ : the equivalent width at the impact parameter  $r/r_{vir} \lesssim 0.5$  for  $M = 10^5 M_\odot$  at  $z = 10$  (solid lines) decreases from  $\sim 0.2$  KHz for the standard recombination to a negligible value  $\lesssim 0.01$  KHz for  $\xi/\xi_L = 1$ . At  $z = 15.5, 12$  (dash and dot-dash lines) the equivalent width shows not such a catastrophic drop, however it hardly can be resolved on future telescopes and deposit into the total signal in broad-band observations (Xu *et al.* 2011).

Lines with equivalent widths  $W_\nu^{obs} \gtrsim 0.2$  KHz can be formed by haloes with  $M \gtrsim 10^6 M_\odot$  at  $z = 10$  (solid lines) for  $\xi/\xi_L \lesssim 0.3$  up to  $\alpha = r/r_{vir} \lesssim 1$ . In the higher redshift range,  $z = 15.5, 12$ , such strong lines can be associated only with  $M \gtrsim 10^6 M_\odot$  in the standard recombination model. Higher equivalent widths  $\sim 0.5 - 0.9$  KHz can be attributed to low impact factors  $\alpha \sim 0.3$  in the standard recombination. However, more massive haloes,  $M = 10^7 M_\odot$ , can form strong absorptions with the width  $\gtrsim 0.5$  KHz even for high ionization rate  $\xi \sim \xi_L$ , though only in a narrow impact factor range  $\alpha \lesssim 0.1$ . Thus, the decaying dark matter leads to a considerable decrease of the number of strong absorption lines. This suppression of the 21 cm absorption is similar to what stems from the action of the X-ray background (Furlanetto & Loeb 2002; Xu *et al.* 2011). For  $\xi/\xi_L \gtrsim 0.3$  strong lines are formed only in high-mass ( $M \sim 10^7 M_\odot$ ) haloes nearly along the diameter, but such events are rarely expected.

The sensitivity of future telescopes is more than one order of magnitude lower than the flux limit needed to separate spectral lines from individual haloes, i.e. to observe with spectral resolution of 1 KHz (Xu *et al.* 2011). Therefore, Xu *et al.* (2011) have proposed broad-band observations with lower resolution. In this case one measures averaged signal from different haloes crossed by a line of sight. Accordingly, we introduce a radially averaged observed equivalent width:  $\langle W_\nu^{obs} \rangle = \int_0^{3r_{vir}} W_\nu^{obs}(r) r dr / r_{vir}^2$ . Figure 8 presents the dependence of this value for minihaloes  $M = 10^5, 10^6 M_\odot, 10^7 M_\odot$  on  $\xi/\xi_L$ . The increase of  $\langle W_\nu^{obs} \rangle$  for  $M = 10^5 M_\odot$  at  $z = 10$  and  $\xi/\xi_L \leq 0.1$  is explained by a widening of  $W_\nu^{obs}$  in the range of impact factor up to  $r/r_{vir} \lesssim 2$  (see upper panels in Figure 7). For other considered masses and redshifts the radially averaged  $W_\nu^{obs}$  decreases when  $\xi/\xi_L$  grows by a factor of 1.2-2, which apparently is sufficient to identify effects from additional ionization sources, and in particular, from decaying DM particles.

In previous studies theoretical spectrum of the 21 cm forest has been simulated within the assumption of steady-state minihaloes with fixed profiles corresponding to the virialization (Furlanetto & Loeb 2002; Xu *et al.* 2011). When dynamics is taken into account, minihaloes lying on a given line of sight are, in general, at different evolutionary stages, and have different density, velocity and temperature profiles. Moreover, Press-Schechter formalism cannot anymore be used for description of their mass function as soon as they are lying far from the virialization. It makes problematic to describe correctly the number density of minihaloes at each evolutionary stage. Possible formation of stars in massive evolved minihaloes brings additional complication. Overall, the analysis of theoretical spectrum within a statistical simulation becomes exceedingly cumbersome. More relevant picture can be obtained from high-resolution cosmo-

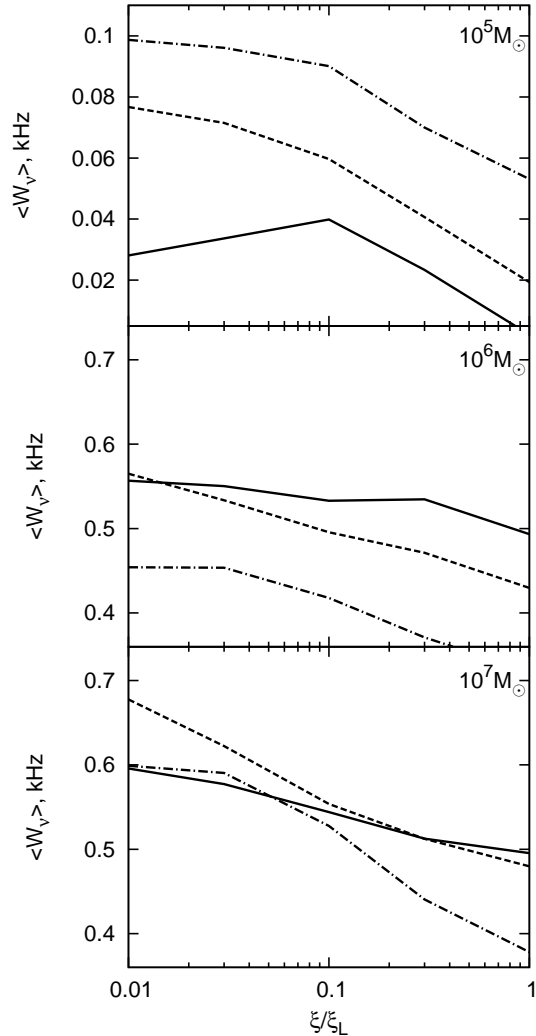


**Figure 8.** The dependence of the radially averaged observed equivalent width for minihaloes with mass  $M = 10^5, 10^6 M_\odot, 10^7 M_\odot$  (from top to bottom panels, correspondingly) at redshifts  $z = 15.5, 12$  and  $10$  (dot-dash, dash and solid lines, correspondingly) on the normalized rate of the decay energy deposited in baryonic gas  $\xi/\xi_L$ , where  $\xi_L = 0.59 \times 10^{-25} \text{ s}^{-1}$ ; in the logarithmic  $x$ -axis  $\xi/\xi_L = 0.01$  is set to correspond to  $\xi/\xi_L = 0$ , i.e. the standard recombination. Note differences between the panels on  $y$ -axes scales.

logical gas dynamic simulation, although current resolution with  $\Delta M \sim 10^6 M_\odot$  seems not to be sufficient.

However, with the upcoming low frequency interferometers (LOFAR and SKA) such modeling seems to be excessive and unnecessary. Indeed, the absorption line profiles and the spectral features from separate minihaloes located at  $z = 10$  are of 1 to 5 KHz in width – close to the resolution limit 1 KHz. As mentioned Xu *et al.* (2011) the sensitivity corresponding to such a resolution requires enormously bright background sources, GRB afterglows and/or QSOs, and broad-band observations can be a better alternative. In broadband observations the suppression of optical depth in 21 cm caused by decaying particles manifests as a factor of 2–4 decrease of absorption in the frequency range  $\nu < 140$  MHz where contribution from low mass mini-

haloes at  $z \gtrsim 10$  dominates. Indeed, the number of haloes in the low-mass range  $10^5 - 10^7 M_\odot$  at  $z = 10$  scales as  $n(M, z) \sim M^{-1}$  (the Press-Schechter mass function). The probability of minihaloes to intersect a line of sight is proportional to  $n(M, z) \times (ar_{vir}(M))^2$ , resulting in a decrease of the number of strong absorption lines with  $W_\nu^{obs} \gtrsim 0.3$  kHz by factor of at least 2.5 for  $\xi/\xi_L = 0.3$  and more than 4.5 for  $\xi/\xi_L = 1$ . Such a decrease inevitably cancels the average 21 cm forest signal from low mass haloes expected in future broadband observations.

## 6 CONCLUSIONS

In this paper we have considered the influence of decaying dark matter particles on the HI 21 cm absorption features from low mass minihaloes with mass  $M = 10^5, 10^6 M_\odot, 10^7 M_\odot$  virialized at  $z_{vir} = 10$ . We used a 1D self-consistent hydrodynamic approach to study their evolution, and followed through the absorption characteristics from the turnaround to the virialization of minihaloes. We have found that

- due to an additional heating brought by decaying particles thermal and dynamical evolution of minihaloes in the presence of decaying dark matter shows considerable difference from that in the model without particle decays (i.e. with the standard recombination scenario);
- this additional heating strongly suppresses optical depth in the 21 cm line: it practically “erases” the 21 cm absorptions from minihaloes with  $M = 10^5 - 10^6 M_\odot$  even at a relatively modest ( $\xi \gtrsim 0.3\xi_L$ ) ionization rate from decaying DM particles; the horn-like dependence of the optical depth found for minihaloes with  $M \sim 10^6 - 10^7 M_\odot$  in the standard recombination scenario Xu *et al.* (2011) almost disappears even at a lower ionization rate  $\xi \gtrsim 0.1\xi_L$ ;
- the equivalent width of the 21 cm absorption line decreases significantly while  $\xi$  increases, and the number of strong absorption lines  $W_\nu^{obs} \gtrsim 0.3$  kHz at  $z = 10$  drops by more than 2.5 to 4.5 times depending on  $\xi$ ; such a decrease inevitably erases the averaged 21 cm forest signal from low mass haloes ( $M \sim 10^6 - 10^7 M_\odot$ , i.e. the frequency range  $\nu < 140$  MHz) in future broad-band observations.

## 7 ACKNOWLEDGEMENTS

This work is supported by the Federal Agency of Education (project codes RNP 2.1.1/11879, P-685). EV acknowledges support from the “Dynasty” foundation.

## REFERENCES

- Bagla J.S., Nath B.B., Padmanabhan T., 1997, MNRAS, 289, 571
- Belikov A. V. & Hooper D., 2009, PhRvD, 80c5007
- Berezinsky V. S., Kachelrieß M. & Vilenkin A., 1997, Phys. Rev. Lett., 79, 4302
- Bharadwaj S. & Sethi S., 1998, ApJS, 114, 37
- Biermann P.L. & Kusenko A. 2006, Phys. Rev. Lett. 96i, 1301
- Birkel M. & Sarkar, S., 1998, Astropart. Phys., 9, 298
- Burkert A., 1995, ApJ, 447, L25
- Carilli C.L., Gnedin N.Y., Owen F., 2002, ApJ, 577, 22
- Cen R., 1992, ApJ, 78, 341
- Cen R., 2006, ApJ, 648, 47
- Chen, X. & Kamionkowski, M., 2004, Phys. Rev. D, 70, 043502
- Chen X. & Miralda-Escudè J., 2004, ApJ, 602, 1
- Chuzhoy L. 2008, ApJL, 679, 65
- Cirelli M., Iocco F., Panci P., 2009, JCAP, 10, 009
- Cumberbatch D. T., Lattanzi M., Silk J., 2010, PhRvD, 82j3508
- DeLope Amigo S., Man-Yin Cheung W., Huang Zh., Ng S.-P., 2009, JCAP, 06, 005
- Dodelson S. & Jubas J.M., 1994, MNRAS, 266, 886
- Doroshkevich A.G. & Naselsky P.D., 2002, Phys. Rev. D, 12, 123517
- Doroshkevich A.G., Naselsky I.P., Naselsky P.D., Novikov I.D., 2003, ApJ, 586, 709
- Field G.B., 1958, Proc. IRE, 46, 240
- Flower D., 2000, MNRAS, 318, 875
- Furlanetto S.R., Loeb A., 2002, ApJ, 579, 1
- Furlanetto S. R., 2006, MNRAS, 370, 1867
- Furlanetto S. R., Oh S. P., Pierpaoli E., 2006a, Phys. Rev. D, 74, 103502
- Galli S., Iocco F., Bertone G., Melchiorri A., 2011, PhRvD, 84b7302
- Galli D. & Palla F., 1998, A&A, 335, 403
- Hansen S. H. & Haiman, Z., 2004, ApJ, 600, 26
- Hogan C.J. & Rees M.J., 1979, MNRAS, 188, 791
- Hütsi G., Chluba J., Hektor A., Raidal M., 2011, A&A accepted arXiv:1103.2766
- Iliev I.T., Shapiro P.R., Ferrara A., Martel H., 2002, ApJL, 572, 123
- Kasuya S. & Kawasaki M., 2004, Phys. Rev. D, 70, 103519
- Kasuya S., Kawasaki M. & Sugiyama, N., 2004, Phys. Rev. D, 69b, 3512
- Kuhlen M., Madau P., Montgomeri R., 2006, ApJL, 637, 1
- Kumar A., Padmanabhan T., Subramanian K., 1995, MNRAS, 272, 544
- Kuzmin V. A. & Rubakov V. A., 1998, Phys. Atom. Nucl., 61, 1028
- Lipovka A., Núñez-López R., Avila-Reese V., 2005, MNRAS, 361, 850
- Liszt H., 2001, A&A, 371, 698
- Mack K. J. & Wyithe J.S.B. 2011, MNRAS submitted, arXiv1101.5431
- Madau P., Meislin A., Rees M.J., 1997, ApJ, 475, 492
- Mapelli M., Ferrara A., Pierpaoli E., 2006, MNRAS 369, 1719
- Mashchenko S., Couchman H.M.P., Wadsley J., 2006, Nature, 442, 539
- Meiksin A., 2011, MNRAS, 417, 1480
- Mikheeva E.V., Doroshkevich A.G., Lukash V.N., 2007, Nuovo Cim. B, 122, 1393
- Myers Z. & Nusser A., 2008, MNRAS, 384, 727
- Natarajan A. & Schwarz D. J. 2009, PhRvD, 80d3529
- Navarro J.F., Frenk C.S., White S.D.M., 1997, ApJ, 490, 493
- Padmanabhan T., 1993, Structure Formation in the Universe, Cambridge Univ. Press, Cambridge
- Peter, A., Moody, C. E., Benson, A. J., Kamionkowski M. 2010, arXiv1011.4970

- Pierpaoli E., *Phys. Rev. Lett.*, 2004, 92, 031301  
Ripamonti E., 2007, *MNRAS*, 376, 709  
Sciama, D. W., 1982, *MNRAS*, 198, 1  
Scott D., Rees M. J., Sciama D., 1991, *A&A*, 250, 295  
Sethi S., 2005, *MNRAS*, 363, 818  
Shaver P. A., Windhorst R. A., Madau P., & de Bruyn A. G., 1999, *A&A*, 345, 380  
Shchekinov Yu. A. & Vasiliev E. O., 2004, *A&A*, 419, 19  
Shchekinov Yu. A. & Vasiliev E. O., 2007, *MNRAS*, 379, 1003  
Shull J.M. & van Steenberg M.E. 1985, *ApJ*, 298, 268  
Spergel D. N., Bean R., Doré O. et al., 2007, *ApJS*, 170, 377  
Stancil P.C., Lepp S., Dalgarno A., 1998, *ApJ*, 509, 1  
Tegmark M., Silk J., Rees M. J., Blanchard A., Abel T., Palla F., 1997, *ApJ*, 474, 1  
Thoul A. & Weinberg D., 1995, *ApJ*, 442, 480  
Tonini C., Lapi A., Salucci P., 2006 *ApJ*, 649, 591  
Tozzi P., Madau P., Meislin A., Rees M.J., 2000, *ApJ*, 528, 597  
Vasiliev E. O. & Shchekinov Yu. A., 2006, *Astr. Rept.*, 50, 778  
Vasiliev E. O. & Shchekinov Yu. A., 2012, *Astr. Rept.*, 89, 99  
Wouthuysen S. 1952, *AJ*, 57, 31  
Xu Y., Ferrara A., Chen X., 2011, *MNRAS*, 410, 2025  
Yuan Q., Yue B., Bi. X.-J., Chen X., Zhang X., 2010, *JCAP*, 10, 023  
Yue B., Ciardi B., Scannapieco E., Chen X., 2009, *MNRAS*, 398, 2122  
Zhang L., Chen X., Kamionkowski M., Si Z.-G., Zheng Zh., 2007, *PhRvD*, 76f1301  
Zhang L., Weniger Ch., Maccione L., Redondo J., Sigl G., 2010, *JCAP*, 06, 027